RSC Advances




ROYAL SOCIETY OF CHEMISTRY

www.rsc.org/advances

RSC Advances RSCPublishing

COMMUNICATION

# Arginine-assisted synthesis of palladium nanochain networks and their enhanced electrocatalytic activity for the borohydride oxidation†

Cite this: DOI: 10.1039/x0xx00000x

Received 00th January 2012
Accepted 00th January 2012

DOI: 10.1039/x0xx00000x

www.rsc.org/

Geng-Tao Fu,[a] Rui Wu,[a] Chang Liu,[a] Jun Lin,[a,b] Dong-Mei Sun,*[a] and Ya-Wen Tang*[a,b]

**We report a one-pot hydrothermal route for the successful preparation of the three-dimensional (3D) Pd nanochain networks by arginine-assisted self-assembly process, which show the higher electrocatalytic activity and stability than commercial Pd black for the borohydride oxidation reaction due to the unique 3D network structure.**

Nowadays, the morphology-controlled synthesis of the precious metal nanocrystals (PMNs) with tailored-shape and -size has received extensive attention, because the catalytic activity and stability of the PMNs strongly depend on their morphologies.[1-12] Currently, various PMNs with different morphologies have been successfully prepared, including zero-dimensional (0D) nanostructures (e.g., spheres and polyhedrons),[1, 2] one-dimensional (1D) nanostructures (e.g., rods and wires/chains)[3, 4] and two-dimensional (2D) nanostructures (e.g., discs and plates).[8, 9] Of particular interest are three-dimensional (3D) network nanostructures consisting of 1D nanochains/wires due to their large surface area and outstanding mass transfer efficiency compared with 0D nanostructures,[4-7, 13, 14] which endow the PMNs with improved activity and stability for many important catalytic/electrocatalytic reactions. Meanwhile, abundant defect sites on the PMNs surfaces, such as steps and kinks, can provide active sites available for the reaction and effectively accelerate the kinetics of catalytic/electrocatalytic reaction.[15, 16]

Thanks to the efforts from many research groups, several significant progresses with regard to 3D nanostructures have been developed using different strategies.[4-7] For example, Xia and co-workers successfully synthesized ultrathin Pd nanowires by using the polyol method without the involvement of any template, which exhibited superior electrocatalytic activity for the formic acid oxidation reaction.[4] More recently, the self-assembled Pt nanochain networks were also successfully prepared in polyvinylpyrrolidone (PVP) solution using in-situ induced magnetic dipoles strategy.[5] To the best of our knowledge, little research focuses on the interrelationship between the formation mechanism of nanochains/wires and the functional groups of structure directing agent employed.

As one of the important energy conversion technologies, direct borohydride fuel cells (DBFCs) have attracted significant interest due to the high hydrogen content (10.6 Wt%), high stability in alkaline medium, non-toxic (i.e., the absence of carbon at $NaBH_4$) and the superior theoretical energy density (9.3 kW·h $kg^{-1}$) compared to direct ethanol (8.01 kW·h $kg^{-1}$), methanol (6.09 kW·h $kg^{-1}$) and formic acid (1.740 kW·h $kg^{-1}$) fuel cells.[17-23] Thus, the development of highly active PMNs electrocatalysts for the borohydride oxidation reaction (BOR) will facilitate the commercialization of DBFCs. Pd, as one of the precious metal, has already been widely applied to borohydride electrocatalytic oxidation due to their excellent electrocatalytic activity and stability in alkaline medium.[21, 24-28]

Herein, we report a facile and environmentally friendly synthetic route for the high-yield preparation of the Pd nanochain networks (Pd-NCNs) using PVP as the reductant and stabilizing agent with the assistance of arginine molecule (see Experimental section for details). Although various Pt-based nanostructures, including Pt concave cubes,[29] Pt-Ni hexoctahedra,[30] and Pt-Cu octahedral frames,[31] have been fabricated in amino acid solution, to the best of our knowledge, the chain-like Pd nanostructures have never been synthesized in the amino acid system. In our synthetic system, the arginine-assisted synthesis in water system provides a environmentally friendly synthetic route for controlling the chain-like shape As expected, the as-prepared Pd-NCNs show superior electrocatalytic activity and stability for the BOR compared to commercial Pd black due to their unique 3D network structure.

In a typical synthesis, the Pd-NCNs were obtained by reducing Pd(II) precursors with PVP as the reductant and stabilizing agent in arginine aqueous solution at 140 $^oC$ for 3 h (see Experimental section for details, ESI†). The morphology and structure of the as-prepared Pd nanocrystals were investigated by transmission electron microscopy (TEM) and scanning electron microscopy (SEM). As observed, the overall morphology of the as-prepared Pd nanocrystals is 3D network-like structure, which is composed of the interconnected 1D Pd nanochains (Fig. 1 A-B). In the whole TEM images, no isolated

nanocrystal is observed, demonstrating that the high-yield formation of the 3D Pd-NCNs. SEM image further clearly confirms that the as-prepared Pd nanocrystals have 3D network-like architectures with abundant secondary pores (Fig. 1C and Fig. S1, ESI†), Such unique 3D networks, consisting of closed interconnected Pd nanocrystals with abundant pores, are believed to be a good candidate for the electrocatalysis, which provide a better mass transport property and higher Pd utilization efficiency.[3, 32, 33] Careful observation find that the nanochain is made up of many Pd nanocrystals with 10.5 nm average diameter as the building blocks, in which the nanocrystals closely connect one-by-one from different angles (Fig. 1D). The corresponding selected area electron diffraction (SAED) pattern (inset in Fig. 1D) highlights not only continuous rings indexed to Pd {111}, {200}, {220}, {311} and {220} facets, but also discrete diffraction spots that comes from the substructure of whole ensemble of nanocrystals, demonstrating the polycrystalline nature. More structural information was further provided by high-resolution TEM (HRTEM) image. There are no gaps between the adjacent Pd nanocrystals (Fig. 1E). Magnified HRTEM images show that the interplanar spacing is 0.225 nm on each Pd nanocrystals surface, corresponding to the lattice spacing of face centered cubic (*fcc*) Pd {111} facets (Fig. 1F and Fig. S2, ESI†). More importantly, a large amount of surface defect sites can be clearly observed on the surface of the nanochains (marked by yellow ellipses).

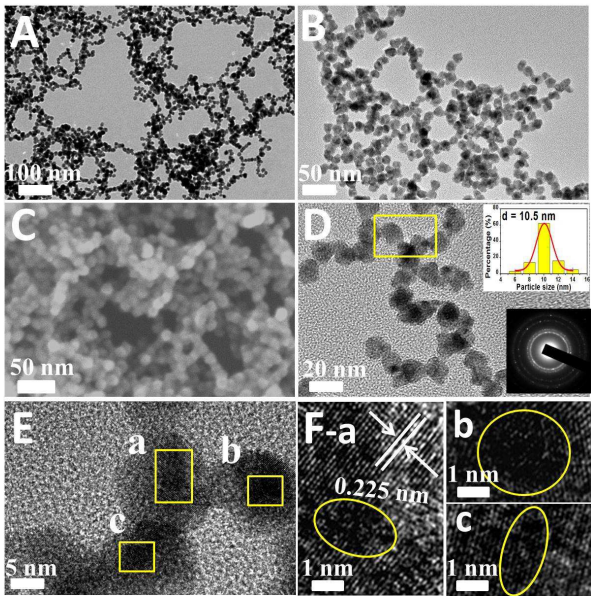


**Fig. 1** (A, B) Typical TEM and (C) SEM images of the Pd-NCNs. (D, E) HRTEM images of the Pd-NCNs. the top-right and bottom-right insets show the corresponding particle-size distribution histogram and SAED pattern, respectively. (F) Magnified HRTEM image taken from regions a, b and c (marked by the squares in D), which correspond to E-a, E-b and E-c, respectively.

The crystal structures, composition and chemical states of the products were analyzed by X-ray diffraction (XRD), energy dispersive X-ray (EDX) and X-ray photoelectron spectroscopy (XPS), respectively. XRD pattern shows that all of the reflections of sample can be indexed to *fcc* Pd (JCPDS card no. 46–1043), showing a high degree of metallic character and crystallinity (Fig. 2A). The broadening of the peaks can be attributed to the small particle size (ca. 10.7 nm), which is calculated from the Scherrer equation.[4, 34] The EDX spectrum reveals intensively Pd signal (Fig. 2B), which is consistent with survey XPS spectrum (Fig. 2C). In the high resolution Pd3d XPS spectrum (Fig. 2D), the doublet peaks at 334.86 eV and 340.12 eV are attributed to the 3d5/2 and 3d3/2 binding energies of the metallic Pd, while the doublet peaks at 336.93 eV and 342.16 eV corresponds to the 3d5/2 and 3d3/2 binding energies of the surface Pd oxide. By measuring the relative peak areas, the percentage of $Pd^0$ species is calculated to be 96.1%, indicating that Pd(II) precursor is successfully reduced to metallic Pd.

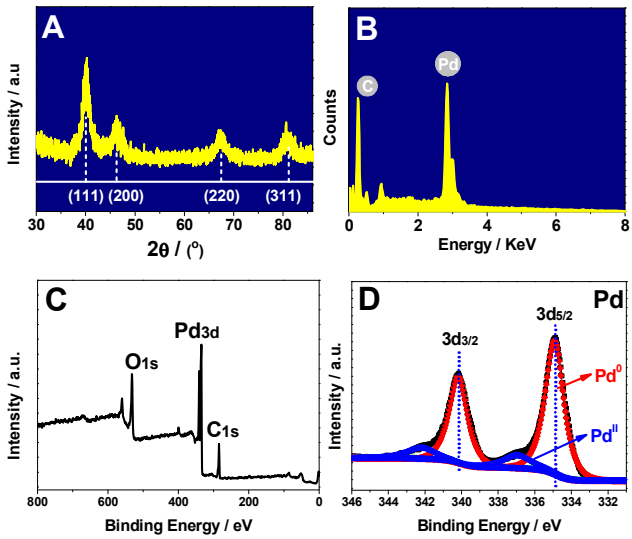


**Fig. 2** (A) XRD pattern and (B) EDX spectrum of Pd-NCNs. XPS spectra of Pd-NCNs: (C) survey scan and (D) high resolution XPS spectrum for element Pd.

To in-depth understand how the Pd-NCNs were formed during reaction process, the time sequential evolution experiments of Pd-NCNs were investigated by TEM. At the initial stage (2 h, Fig. 3A), some small Pd nanocrystals generate, the partial Pd nanocrystals start to assemble with each other to generate short nanochains (note: the products are hardly collected within 2 h). With the increase of reaction time (2.5 h, Fig. 3B), the short nanochains further self-assemble end-to-end to generate elongated nanochains, and the isolated Pd nanocrystals disappear. At 3 h, the Pd nanochains reach their max-length (Fig. 3C), and remain unchanged even for prolonged time (Fig. 3D). During the evolution/growth process, the particle size of each nanocrystals almost doesn't change, suggesting that Pd-NCNs grow from the primary nanocrystals through the oriented self-assembled attachment.[4, 7, 35, 36]

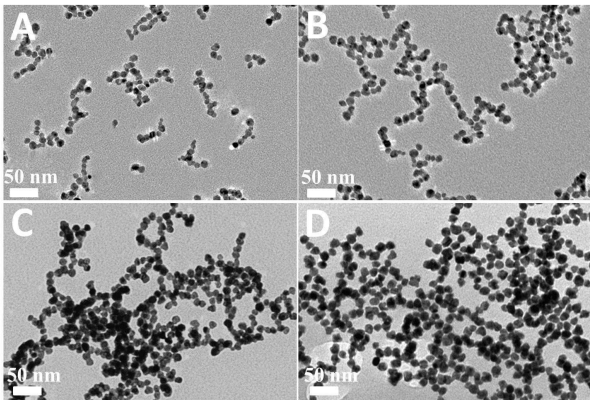


**Fig. 3** TEM images of Pd-NCNs synthesized at a reaction time of (A) 2 h, (B) 2.5 h, (C) 3 h, and (D) 4 h.

We further investigated the possible roles of PVP and arginine molecules for the formation of the Pd-NCNs by TEM. Previous works show the PVP molecules could be successfully employed to direct the growth of chain-like metal nanocrystals, because of itself chain-like structure.[37, 38] In order to confirm whether PVP molecules drive the formation of Pd nanochain, a controlled experiment was performed under the same conditions with the exception of the absence of arginine molecule (Fig. 4A). Unfortunately, the irregular and small Pd nanocrystals are obtained, instead of Pd nanochains. This observation indicates PVP doesn't make important contributions to direct the formation of chain-like shape in our synthesis. When only arginine molecule is used (i.e., without PVP), a large number of large-sized Pd nanochains are achieved (Fig. 4B), indicating the introduction of arginine is a key factor for the formation of the Pd-NCNs. In conjunction with these results, PVP is thought to function as the reductant and stabilizing agent, whereas arginine mainly acts as the structure-directing agent and co-reductant under the present conditions.

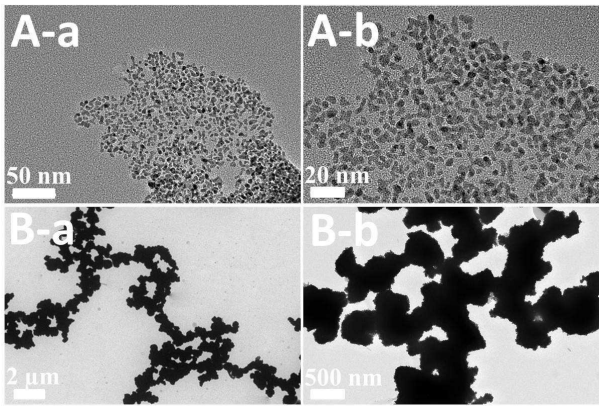


**Fig. 4** TEM images of Pd nanocrystals prepared under the same conditions as in Fig. 1 with the exception of the absence of (A) arginine and (B) PVP molecules.

Considering the presence of abundant amino and carboxyl groups in arginine molecule (Scheme S1, ESI†), we presume that the synergetic interactions between amino groups and carboxyl groups, including hydrogen-bonding interaction andelectrostatic interaction,[39-41] may be the primary driving force for the formation of chain-like nanostructures. Specifically, the formation of Pd-NCNs involves the following main processes: i) the generation of isolated Pd nanocrystals through the slow kinetics growth, in which the amino acid strongly binds on the surface of preformed Pd nanocrystals due to the particular coordination interaction between amino acid and $Pd^{II}$;[42] ii) the self-connection of the isolated Pd nanocrystals, in which the synergetic interactions between amino groups and carboxyl groups on isolated nanocrystals drive the connection of two nanocrystals to generate nanochains (Scheme 1).

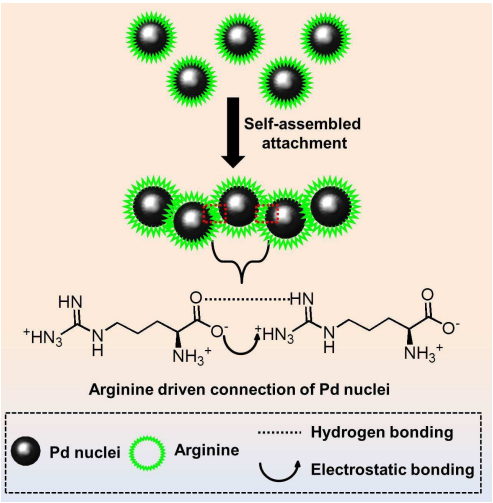


**Scheme 1**. Proposed Mechanism for the Arginine-Based Assembly of detached Pd nanocrystals.

To confirm the function of amino and carboxyl groups, a set of controlled experiments based on the standard procedure were conducted. Firstly, we introduce the same molar amount of ethylamine or acetic acid to substitute arginine in our synthetic system, respectively. As expected, no Pd nanochains are obtained (Fig. 5A-B). Alternatively, when L-lysine (Scheme S2, ESI†), one of amino acid homologues, is used instead of arginine, Pd nanochains are also obtained (Fig. 5C). Thus, it can be concluded that the synergetic effect of amino groups and carboxyl groups helps to drive the formation of the Pd nanochains.

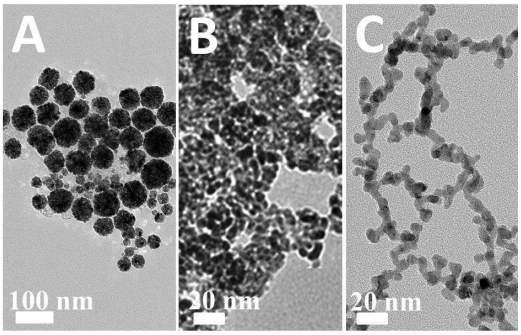


**Fig. 5** TEM images of Pd nanocrystals prepared under the same conditions as in Fig. 1, except the use of other reagents instead of arginine: (A) ethylamine, (B) acetic acid, and (C) L-lysine.

Since the Pd-NCNs have special 3D network structure, the enhanced catalytic/electrocatalytic performance was expected. Herein, the electrochemical performance of Pd-NCNs was investigated. For comparison, a commercial Pd black was employed as a benchmark material. According to cyclic voltammetry (CV) curves of Pd-NCNs and commercial Pd black recorded in $N_2$-purged 3.0 M NaOH solution at room temperature, the electrochemical active surface area (ECSA) of Pd-NCNs is calculated to be 9.6 $m^2\ g^{-1}$ from the charge of reduction monolayer in Pd oxide region with an assumption of 420 $\mu C\ cm^{-2}$ (see Experimental section for details), which is larger than that of commercial Pd black (7.02 $m^2\ g^{-1}$). The electrocatalytic activities of Pd-NCNs and commercial Pd black for the BOR were first evaluated by CV, where the currents were normalized with respect to Pd mass (Fig. 6B). It is well know that the electrochemical behaviour of $BH_4^-$ on the Pd surface are fairly complex and characterized by several oxidation peaks.[24, 25] In the forward scan, the first anodic peak (P1) at ca. −0.35 V can be attributed to the oxidation of $H_2$ generated in the catalytic hydrolysis of $BH_4^-$; The second anodic peak (P2) at ca.−0.18 V can be assigned to direct potentially eight-electron oxidation of $BH_4^-$ (i.e., $BH_4^-+8OH^-\rightarrow BO_2^-+6H_2O+8e^-$), and the unusual reaction pathway is similar with previous studies.[24, 25] As observed, the (P2) peak current (1.03 A $mg^{-1}$) of the BOR on Pd-NCNs is much higher than that (0.60 A $mg^{-1}$) on commercial Pd black (Fig. 6B). In addition, the specific activity (i.e., the current densities were normalized with respect to ECSA) of Pd-NCNs for the BOR is higher than that of commercial Pd black (Fig. 6C), indicating that Pd-NCNs hold promise as potentially practical electrocatalysts for the BOR.

During the BOR, a large amount of hydrogen ($H_2$) may be produced from the $NaBH_4$ hydrolysis ($BH_4^-+2H_2O=4H_2+BO_2^-$), and accumulate on Pd surface to form gas bubbles, which will block the active sites of Pd electrocatalyst.[21] Compared with the commercial Pd black, the as-prepared Pd-NCNs are better for the removal of adsorbed $H_2$ bubbles and liberate more active site due to the unique 3D network structure. Meanwhile, the unique 3D network structure also provides much more active center for electrocatalytic oxidation due to high specific surface area and abundant surface defect sites, which is also responsible for the improved electrocatalytic activity of Pd-NCNs for the BOR. In addition, the electrocatalytic activity of the L-lysine-directed Pd-NCNs towards the BOR was also measured. As observed, the oxidation peak current density (P2) on L-lysine-directed Pd-NCNs is much higher than that on Pt black, and close to the arginine-directed Pd-NCNs (Fig. S3, ESI†), indicating that unique 3D network structure of Pd-NCNs is the key factor for the enhanced electrocatalytic activity.

Besides the activity, the long-term stability of the electrocatalyst is another important parameter in determining its potential application. The durabilities of Pd-NCNs and commercial Pd black for the BOR were evaluated by chronoamperometry at −0.2 V potential in $N_2$-saturated 3.0 M KOH + 0.03 M $NaBH_4$ solution. After running 3000 s, the current of the BOR on Pd-NCNs (23.1 mA $mg^{-1}$) is 2.2 times higher than that on commercial Pd black (10.6 mA $mg^{-1}$), indicating Pd-NCNs have better stability than commercial Pd black for the BOR. The enhanced stability of Pd-NCNs is attributed to the inetrconnected network structure, in which no isolated Pd nanocrystal exists, which effectively restrain the Ostwald ripening and consequently decrease the loss of ECSA. As confirmed, the chain-like shape of Pd-NCNs essentially retains after the chronoamperometry test (Fig. S3, ESI†).

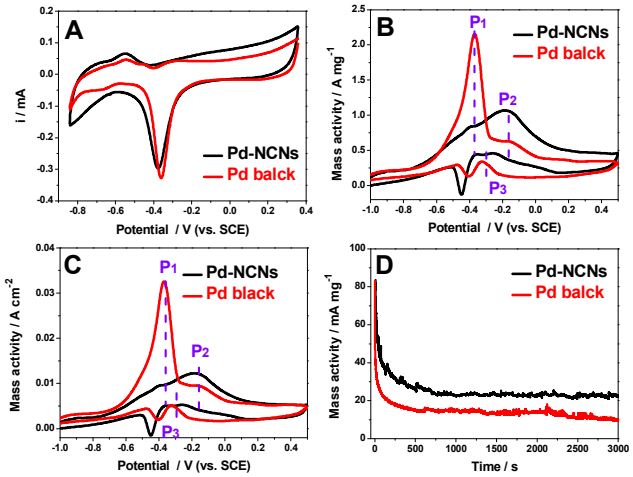


**Fig. 6** (A) The cyclic voltammograms for Pd-NCNs and commercial Pd black in $N_2$-saturated 3.0 M NaOH solution at the scan rate of 50 mV $s^{-1}$. (B) The mass-normalized and (C) ESCA-normalized cyclic voltammograms for Pd-NCNs and commercial Pd black in $N_2$-saturated 3.0 M KOH + 0.03 M $NaBH_4$ solution at the scan rate of 50 mV $s^{-1}$. (D) Chronoamperometry curves for Pd-NCNs and commercial Pd black in $N_2$-saturated 3.0 M KOH + 0.03 M $NaBH_4$ solution for 3000 s at -0.20 V potential.

## Conclusions

In summary, for the first time, we have developed a simple arginine-assisted hydrothermal route to produce Pd-NCNs in the presence of PVP. In the synthesis, arginine molecules mainly act as structure directing agent and co-reductant, and PVP is thought to function as a reductant and stabilizing agent. Through the time sequential evolution experiments and a series of controlled experiments, the possible formation mechanism is presented. Additionally, the obtained Pd-NCNs showed excellent electrocatalytic activity and stability for the BOR, which is attributed to the unique structure and abundant surface atom defects on Pd-NCNs.

## Acknowledgments

National Natural Science Foundation of China (21376122, 21273116), the United Fund of NSFC and Yunnan Province (U1137602), the National Basic Research Program of China (973 Program, 2012CB215500), Industry-Academia Cooperation Innovation Fund Project of Jiangsu Province (BY2012001 and BY2013001-04), a project funded by the Priority Academic Program Development of Jiangsu Higher Education Institutions, National and Local Joint Engineering Research Center of Biomedical Functional Materials.

## Notes and references

[a] Jiangsu Key Laboratory of New Power Batteries, Jiangsu Collaborative Innovation Center of Biomedical Functional Materials, School of Chemistry and Materials Science, Nanjing Normal University, Nanjing 210023, P. R. China.
[b] Polypeptide drug and their derivatives engineering research center of Jiangsu Province, Jiangsu, P. R. China.

Fax: +86–25–83243286; Tel: +86–25–85891651;
E–mail: sundongmei@njnu.edu.cn (D. Sun)
tangyawen@njnu.edu.cn (Y. Tang)

† Electronic Supplementary Information (ESI) available: Additional characterization data. See DOI: 10.1039/b000000x/

1. H. Huang, Y. Wang, A. Ruditskiy, H.-C. Peng, X. Zhao, L. Zhang, J. Liu, Z. Ye and Y. Xia, *ACS Nano*, 2014, **8**, 7041-7050.
2. S. I. Lim, I. Ojea-Jiménez, M. Varon, E. Casals, J. Arbiol and V. Puntes, *Nano Lett.*, 2010, **10**, 964-973.
3. Y. Tang, R. E. Edelmann and S. Zou, *Nanoscale*, 2014, **6**, 5630-5633.
4. Y. Wang, S. I. Choi, X. Zhao, S. Xie, H. C. Peng, M. Chi, C. Z. Huang and Y. Xia, *Adv. Funct. Mater.*, 2014, **24**, 131-139.
5. M. R. Gao, S. R. Zhang, Y. F. Xu, Y. R. Zheng, J. Jiang and S. H. Yu, *Adv. Funct. Mater.*, 2014, **24**, 916-924.
6. Y. Song, R. M. Garcia, R. M. Dorin, H. Wang, Y. Qiu, E. N. Coker, W. A. Steen, J. E. Miller and J. A. Shelnutt, *Nano Lett.*, 2007, **7**, 3650-3655.
7. J. Xu, G. Fu, Y. Tang, Y. Zhou, Y. Chen and T. Lu, *J. Mater. Chem.*, 2012, **22**, 13585-13590.
8. M. Maillard, P. Huang and L. Brus, *Nano Lett.*, 2003, **3**, 1611-1615.
9. B. Lim, J. Wang, P. H. Camargo, M. Jiang, M. J. Kim and Y. Xia, *Nano Lett.*, 2008, **8**, 2535-2540.
10. M. Chen, B. Wu, J. Yang and N. Zheng, *Adv. Mater.*, 2012, **24**, 862-879.
11. S. Yang and X. Luo, *Nanoscale*, 2014, **6**, 4438-4457.
12. H. You, S. Yang, B. Ding and H. Yang, *Chem. Soc. Rev.*, 2013, **42**, 2880-2904
13. Y. Xu, R. Xu, J. Cui, Y. Liu and B. Zhang, *Chem. Commun.*, 2012, **48**, 3881-3883.
14. L. Ye, Y. Wang, X. Y. Chen, B. Yue, S. C. Tsang and H. Y. He, *Chem. Commun.*, 2011, **47**, 7389-7391.
15. Z. Niu, D. Wang, R. Yu, Q. Peng and Y. Li, *Chem. Sci.*, 2012, **3**, 1925-1929.
16. G. Fu, Z. Liu, Y. Chen, J. Lin, Y. Tang and T. Lu, *Nano Res.*, 2014, **7**, 1205-1214.
17. S. C. Amendola, P. Onnerud, M. T. Kelly, P. J. Petillo, S. L. Sharp-Goldman and M. Binder, *J. Power Sources*, 1999, **84**, 130-133.
18. G. Rostamikia and M. J. Janik, *Energy Environ. Sci.*, 2010, **3**, 1262-1274.
19. M. Simoes, S. Baranton and C. Coutanceau, *J. Phys. Chem. C*, 2009, **113**, 13369-13376.
20. D. Zhang, K. Ye, J. Yin, K. Cheng, D. Cao and G. Wang, *New J. Chem.*, 2014, **38**, 5376-5381.
21. K. Cheng, D. X. Cao, F. Yang, L. L. Zhang, Y. Xu and G. L. Wang, *J. Mater. Chem.*, 2012, **22**, 850-855.
22. A. Serov, A. Aziznia, P. H. Benhangi, K. Artyushkova, P. Atanassov and E. Gyenge, *J. Mater. Chem. A*, 2013, **1**, 14384-14391.
23. W. Hong, J. Wang and E. Wang, *ACS Appl. Mater. Interfaces*, 2014, **6**, 9481–9487
24. J. Q. Yang, B. H. Liu and S. Wu, *J. Power Sources*, 2009, **194**, 824-829.
25. G. Behmenyar and A. N. Akin, *J. Power Sources*, 2014, **249**, 239-246.
26. K. Cheng, D. Cao, F. Yang, D. Zhang, P. Yan, J. Yin and G. Wang, *J. Power Sources*, 2013, **242**, 141-147.
27. K. Cheng, Y. Xu, R. R. Miao, F. Yang, J. L. Yin, G. L. Wang and D. X. Cao, *Fuel Cells*, 2012, **12**, 869-875.
28. M. Simoes, S. Baranton and C. Coutanceau, *Electrochim. Acta*, 2010, **56**, 580-591.
29. Z. C. Zhang, J. F. Hui, Z. C. Liu, X. Zhang, J. Zhuang and X. Wang, *Langmuir*, 2012, **28**, 14845-14848.
30. X. Xu, X. Zhang, H. Sun, Y. Yang, X. Dai, J. Gao, X. Li, P. Zhang, H. H. Wang and N. F. Yu, *Angew. Chem. Int. Edit.*, 2014, **126**, 12730-12735.
31. X. Wang, F. Nosheen, Z. C. Zhang and J. Zhuang, *Nanoscale*, 2013, **5**, 3660-3663.
32. Y. Xu, R. Xu, J. H. Cui, Y. Liu and B. Zhang, *Chem. Commun.*, 2012, **48**, 3881-3883.
33. D. Y. Kim, S. W. Kang, K. W. Choi, S. W. Choi, S. W. Han, S. H. Im and O. O. Park, *CrystEngComm*, 2013, **15**, 7113-7120.
34. G. Fu, K. Wu, J. Lin, Y. Tang, Y. Chen, Y. Zhou and T. Lu, *J. Phys. Chem. C*, 2013, **117**, 9826-9834.
35. M. Xiao, S. Li, J. Zhu, K. Li, C. Liu and W. Xing, *ChemPlusChem*, 2014, **79**, 1123–1128.
36. Z. M. Peng, H. J. You and H. Yang, *ACS nano*, 2010, **4**, 1501-1510.
37. D. F. Zhang, L. Y. Niu, L. Jiang, P. G. Yin, L. D. Sun, H. Zhang, R. Zhang, L. Guo and C. H. Yan, *J. Phys. Chem. C*, 2008, **112**, 16011-16016.
38. L. Guo, F. Liang, X. Wen, S. Yang, L. He, W. Zheng, C. Chen and Q. Zhong, *Adv. Funct. Mater.*, 2007, **17**, 425-430.
39. S. H. Choi, S. H. Lee, Y. M. Hwang, K. P. Lee and H. D. Kang, *Radiat. Phys. Chem.*, 2003, **67**, 517-521.
40. Z. Gu, R. Zambrano and A. McDermott, *J. Am. Chem. Soc.*, 1994, **116**, 6368-6372.
41. H. Ahn, T. Kim, H. Choi, C. Yoon, K. Um, J. Nam, K. H. Ahn and K. Lee, *Carbon*, 2014, **71**, 229-237.
42. G. Fu, X. Jiang, R. Wu, S. Wei, D. Sun, Y. Tang, T. Lu and Y. Chen, *ACS Appl. Mater. Interfaces*, 2014, **6**, 22790-22795.